CAVITATING FLOW PAST A CASCADE OF CIRCULAR ARC HYDROFOILS

by

A. J. Acosta

Division of Engineering
California Institute of Technology

March 1960
Report E-79.2

Notation

A, B, D, E, G	Constants
a	Eq. (11a)
c	Chord (dimensionless)
c_p	pressure coefficient (Eq. 2a)
C_N	normal force coefficient (Eq. 21)
C_D	drag coefficient
i	$\sqrt{-1}$
k	cavitation number (Eq. 1)
p	pressure
t	auxiliary mapping plane (Eq. 8)
u	velocity component in x direction
v	velocity component in y direction
V	magnitude of velocity
w	$u - iv$, complex velocity function
x, y	coordinates of physical plane
z	$x + iy$
α	flow angle with respect to the chord
γ	stagger angle
ζ	auxiliary transformation plane (Eq. 9)
η	coordinate of wetted surface
σ	solidity $= c/2\pi$
Ω	camber of profile (rad.)
λ	parameter in t plane
$(\ )_1$	denotes far upstream of cascade
$(\ )_2$	denotes far downstream of cascade
$(\ )'$	denotes perturbation quantity
$\overline{(\ )}$	denotes conjugate quantity

Cavitating Flow Past a Cascade of Circular Arc Hydrofoils

I. Introduction

Continued interest in the application of cavitating hydrofoils to various types of lifting and control surfaces on water craft, the recently publicized super-cavitating propeller and other types of rotating machinery, has resulted in a considerable amount of information on the behavior of the cavitating flow past isolated objects. The flow details of many configurations of interest may not, however, be approximated well by information on isolated shapes. For example, the close proximity of the neighboring vanes in a lifting ladder foil used for the support of a hydrofoil boat might conceivably have an important effect on the lift of an individual blade. The same effect may be expected to occur in the flow through the blades of a propeller with extensive cavitation. The problem of the cavitating flow through a cascade or lattice of hydrofoils is then of considerable technical interest, although only a few works have appeared on this subject.

The case of free streamline flow through a cascade of flat plate hydrofoils with infinitely long cavities was first treated by Betz and Petersohn*(1) with the aid of the hodograph method. They were able to include in a simple way variable angle of attack and stagger angle. Their work was used subsequently by Cornell(2) to calculate loss coefficients (by momentum considerations) for various cascade geometries. Birkhoff and Zarantonello in their book "Jets, Wakes and Cavities"** mention the Betz and Petersohn work and also discuss possible extension of this theory. Calculations of the cavitating flow through cascades of curved hydrofoils

* Numbers in parenthesis refer to the references at the end of the text.
** Academic Press, 1958

and past arbitrary isolated shapes by hodograph techniques appear to be fairly complex, however. For this reason, workers in this field have recently made considerable use of linearization techniques to solve certain types of free streamline problems about "slender" bodies. This approach (first used by M. P. Tulin[3]) embodies in most respects the same assumptions as thin airfoil theory. Linearized free streamline flow problems, however, involve the solution of mixed boundary value problems in contrast to most applications of thin airfoil theory. A recent comprehensive summary of two-dimensional linearized free streamline flow problems and the various techniques used for their solution is due to B. R. Parkin[4]. A more readily available paper containing an example of this method is that of Cohen and Gilbert [5].

The linearized theory is in most cases considerably more simple to use than exact hodograph methods. This advantage is partially offset by loss of accuracy, and in any specific situation it is always desirable to have an estimate of the validity of the solution. Nevertheless, as reference to (4) will show, the linearized method has considerable utility.

The first publication of linearized free-streamline flow through a cascade appeared in 1958 and is due to Cohen and Sutherland[6]. They treat the flow through a cascade of flat plates with arbitrary cavitation number provided the cavities are longer than the chord. As a feature of the problem, the cavity length is fixed when the geometry, cavitation number (Eq. 1) and angle of attack are specified. As in the case of any confined cavitating flow with a given geometry, the cavity length becomes infinite when a certain minimum cavitation number is reached. In this event, the boundaries of the cavity become parallel far from the body, thus limiting

the rate of flow for a given upstream pressure. In analogy to supersonic flow, this limiting case may be called "choked" flow. For this condition, Cohen and Sutherland compare the inlet angle vs. the leaving angle of a flat plate cascade with similar calculations taken from the hodograph theory of Betz and Petersohn and report excellent agreement. Detailed comparison of normal force coefficients is not made, however. Also, they point out that it is possible to formulate solutions by use of integral techniques for any shape of hydrofoil. Unfortunately, the resulting integrals are difficult to evaluate, and in (6) only the case of flat blades is considered. Circular arc hydrofoils show definite advantages over flat plates, and in the present work the choked-cavity flow of a cascade of circular arc profiles is considered. The treatment is similar to that of Cohen and Sutherland. However, the present solution relies on the use of images to obtain results in closed form. Although only the case of circular-arc hydrofoils with infinitely long cavities is worked out in detail, the method can be used for arbitrary cavitation number as well as higher order hydrofoil shapes such as cubic, quartic, etc. In addition, some of the details of the linearization procedure in the present work are slightly different than that of Cohen and Sutherland, and although the differences are slight for small stagger angles, they are apparent for large stagger angles.

II. Formulation of Problem

Figure 1 shows a cavitating cascade composed of circular arc blades with stagger angle γ and solidity σ ($\sigma = 2r/c$). The flow upstream

of the cascade approaches the chord line of the profile at an angle α_1 and is of magnitude V_1. Far downstream, the flow is inclined at angle α_2 to the chord, and since only the fully choked case is considered, the velocity there is taken to be V_2 (greater than V_1). The width of the jets is determined by the continuity equation once V_1, V_2, α_1, and α_2 are known. It is assumed that the slope of the free and "wetted" streamlines of the hydrofoil are small compared to unity. A further restriction is that the width of the cavity must be small compared to the blade spacing. The boundary conditions along the wetted profile and free streamlines are then applied on each of the semi-infinite slits in the cascade (Fig. 2). At the present stage, it is arbitrary whether this slit is aligned with the chord line or with the ultimate direction of the cavity flow. It is probably best to orient the slit with the ultimate cavity direction, although in the present case, it is taken to be along the chord line for convenience in subsequent numerical work. The stagger angle γ is defined in accordance with its usual geometric meaning to be the angle between the cascade axis and the normal to the chord. Thus, the normal to the slit is inclined at the angle γ to be cascade axis as shown in Fig. 2. Had the direction of the slit been chosen to be in agreement with the cavity direction, the normal to the slit would have been inclined at the angle $\gamma + \alpha_2$ to the cascade axis.

The velocity V_2 on the cavity is taken to be the "characteristic" velocity in the vicinity of the cavitating hydrofoil. The connection between V_2, V_1 and the cavitation number is given by Bernoulli's equation

$$K = \frac{p_1 - p_2}{\rho V_1^2/2} = \left(\frac{V_2}{V_1}\right)^2 - 1 \qquad (1)$$

It is convenient to form the pressure coefficient with respect to the cavity pressure p_2, i.e.,

$$c_p = (p-p_2)/\ 1/2\rho V_1^2 = (V_2^2-v^2)/V_1^2 \qquad (2a)$$

Thus, on the cavity $c_p = 0$ and $V = V_2$. The components of the velocity vector V can be written in symbolic form as

$$V = (u, v) = (V_2 \cos \alpha_2 + u', V_2 \sin \alpha_2 + v')$$

where u', v' are perturbation velocities in directions parallel to and perpendicular to the slit. In terms of the perturbation components the pressure coefficient becomes

$$-c_p = (2V_2 \cos \alpha_2 u'^2 + u'^2 + 2V_2 \sin \alpha_2 v' + v'^2)/V_1^2 \qquad (2b)$$

The "slender" property of the flow is now invoked so that the product $\alpha_2 v'$ and v'^2 are each assumed negligible in comparison to V_1^2. The pressure coefficient is then

$$c_p = -\frac{2V_2 \cos \alpha_2 u'}{V_1^2} \qquad (3)$$

Thus, within the limitations of the linearized theory, $c_p = 0$ when $u' = 0$.

It will be seen that for the flow past a flat plate, $v' = O(\alpha_2)$, so that terms of order $(\alpha_2)^2$ are neglected in the pressure formula (2b). (Had the slit been chosen along the ultimate jet direction the term $2V_2 \sin \alpha_2 v'$ would disappear from the pressure equation, but it would still be necessary to drop terms of order $(\alpha_2)^2$.) In any case, however, $\cos \alpha_2$ can be replaced by unity in (3) to the degree of approximation of the present theory. The contour of the wetted surface is then given by the approximate expression

$$\frac{d\eta}{dx} = \frac{v}{V_2} = \frac{V_2 \sin \alpha_2 + v'}{V_2} \tag{4}$$

The boundary conditions can now be explicitly outlined:

$$\left.\begin{array}{ll} \text{(i)} & \text{On the cavity } u' = 0 \\ \text{(ii)} & \text{On the wetted surface } v' = V_2 \frac{d\eta}{dx} - V_2 \alpha_2 \\ \text{(iii)} & \text{The velocity must be non-singular except possibly at the leading edge.} \\ \text{(iv)} & \text{At upstream infinity the vector velocity is } u - iv = V_1 e^{-i\alpha}. \end{array}\right\} \tag{5}$$

Conditions (i) through (iv) are sufficient to determine the flow field in the vicinity of the hydrofoil and at conditions far downstream where $u - iv = V_2 e^{-i\alpha_2}$.

III. Boundary Conditions for a Circular Arc Profile

The profile slope of a circular arc blade is

$$\frac{d\eta}{dx} = \Omega \left(\frac{1}{2} - \frac{x}{c}\right) \tag{6a}$$

where Ω is the total camber and c is the chord, and the coordinate x is measured from the leading edge. Condition (ii) now becomes

$$v' = V_2 \Omega \left(\frac{1}{2} - \frac{x}{c}\right) - V_2 \alpha_2 . \tag{6b}$$

IV. Solution

The solution is obtained with the aid of conformal mapping. The infinite array of semi-infinite slits in the physical (z) plane is mapped onto the upper half of the t plane in such a way that the slit lies along the real axis with the branch point of the slit at the origin in the t plane. A certain length λ of the negative portion of the real t axis represents the

chord in the physical plane. By means of a Joukowsky transformation and suitable translations, this length is transformed into the upper half of the unit circle in the ζ plane. The remainder of the real t axis (corresponding to the cavity) is transformed onto the real ζ axis exterior to the unit circle. The point represented by $z = -\infty$ is designated by $t_{-\infty}$ in the t plane and by ζ_1 in that plane. These details are shown in Fig. 3.

The sequence of mappings described above is

$$z = e^{i\gamma} \ln\left\{1 - te^{i\left(\frac{\pi}{2} - \gamma\right)}\right\} + e^{-i\gamma} \ln\left\{1 - te^{i\left(\frac{\pi}{2} - \gamma\right)}\right\} \qquad (7)$$

and

$$t = \frac{\lambda}{2}\left\{\frac{1}{2}\left(\zeta + \frac{1}{\zeta}\right) - 1\right\} = \frac{\lambda}{4\zeta}\left\{1 - 2\zeta + \zeta^2\right\} \qquad (8)$$

It is seen that (7) maps the real t axis into the array of horizontal slits of slat spacing 2π with the cascade axis inclined at the angle $(-\gamma)$ to the vertical. In the upper half t plane the point $t = e^{i(\pi/2 - \gamma)} = t_{-\infty}$ represents the point $z = -\infty$. When this point ($t_{-\infty}$) is encircled once in the counter-clockwise direction, the argument of z is increased by $2\pi e^{i(\pi/2-\gamma)}$ to progress from one step of the cascade to another. The point $z = +\infty$ is given by $t = \infty$. The length of the chord c is related to the parameter λ by substituting $t = -\lambda$ into (7). The result is

$$\sigma = \frac{c}{2\pi} = \frac{1}{2\pi}\left\{\cos\gamma \ln(1 + \lambda^2 + 2\lambda\sin\gamma) - 2\sin\gamma \tan^{-1}\frac{\lambda\cos\gamma}{1 + \lambda\sin\gamma}\right\} \qquad (9)$$

Equation (7) is a special case of a well-known transformation that maps a cascade of finite slits into the upper half plane. For example, König[7] used this latter transformation in his study of fully wetted flow through a series of flat plate airfoils, and it is the same (to within a constant) as that used by Cohen and Sutherland in their work on finite cavity

cascade flow.

The solution of boundary values (5) is best carried out in the semi-circle plane, and for this purpose it is convenient to combine (7) and (8) in the form

$$z = e^{i\gamma} \ln\left[\frac{-\bar{a}}{\zeta}(\zeta-\zeta_1)(\zeta-\zeta_2)\right] + e^{-i\gamma} \ln\left[\frac{-a}{\zeta}(\zeta-\zeta_1)(\zeta-\zeta_2)\right] \quad (10)$$

where

$$a = \frac{\lambda}{4} e^{-i\left(\frac{\pi}{2}-\gamma\right)} \quad (11a)$$

$$\zeta_1 = \frac{1}{2a}\left[1 + 2a + \sqrt{1+4a}\right] \quad (11b)$$

$$\zeta_2 = \frac{1}{2a}\left[1 + 2a - \sqrt{1+4a}\right] \quad (11c)$$

The form of (10) now conceals the fact that when ζ is on the unit circle $z = x$. In these expressions ζ_1 and ζ_2 are the roots of the equation $\zeta^2 - \frac{1+2a}{a}\zeta + 1 = 0$ and the point ζ_1 corresponds to $z = -\infty$, and is exterior to the unit circle. ζ_2 also corresponds to $z = -\infty$, but is within the unit circle.

As a preliminary step to writing out the solution in full, the non-singular solution for the boundary value problem $v = -x$ on the wetted surface and $u = 0$ on the cavity will be obtained. The basis of the method lies in the realization that the transformation function itself, Eq. (10), contains the desired functional behavior of the solution. For example, consider the relation

$$w_1 = u_1 - iv_1 = iz \quad (12)$$

On the unit circle and real ζ axis, $u = 0$ and $v = -x$ as desired. However, w_1 has logarithmic singularities at ζ_1 and $\zeta = \infty$, and does not therefore represent the desired flow. Fortunately, these singularities

can be removed by subtracting the singular terms in the region exterior to the unit circle from (10). Furthermore, one is still at liberty to add terms regular in this region as long as the constancy of horizontal velocity on the cavity and boundary conditions on the wetted portion of the foil are preserved. These considerations lead to the following velocity function w_2:

$$w_2 = u_2 - iv_2 = w_1 - i\left\{e^{+i\gamma}\ln(\zeta-\bar{\zeta}_1)+e^{-i\gamma}\ln(\zeta-\zeta_1)-e^{-i\gamma}\ln\left(\frac{1}{\zeta}-\zeta_1\right)-e^{+i\gamma}\ln\left(\frac{1}{\zeta}-\bar{\zeta}_1\right)\right\} \tag{13}$$

On the unit circle the added terms are purely real so that $v_2 = -x$ there. On the real ζ axis (or cavity) the added terms are purely imaginary so that u_2 is zero there. Finally, it can be seen upon reference to Eq. (10) that the logarithmic singularities at ζ_1 and infinity are cancelled out. w_2 is therefore regular in the region of the upper half plane exterior to the unit circle and is the solution of the mixed boundary value problem outlined above. The fact that w_2 is regular in the desired region is brought out more clearly by substitution of (10) into (12) and (13) to obtain

$$w_2 = i\left\{2e^{i\gamma}\ln\frac{\zeta-\bar{\zeta}_2}{\zeta}+2e^{-i\gamma}\ln\frac{\zeta-\zeta_2}{\zeta}+G\right\} \tag{14a}$$

where G is the real constant

$$G = e^{i\gamma}\ln\bar{a}\bar{\zeta}_1 + e^{-i\gamma}\ln a\,\zeta_1 \tag{14b}$$

For the purpose of numerical work, G is written out in a form suitable for calculation:

$$G = -2\cos\gamma\ln^2+\cos\gamma\ln\left\{1+\lambda\sin\gamma+\frac{\lambda^2}{4}+(1+2\lambda\sin\gamma+\lambda^2)^{1/4}\left(2\cos\frac{\theta_1}{2}+\lambda\sin\left(\gamma+\frac{\theta_1}{2}\right)\right.\right.$$
$$\left.\left.+(1+2)\lambda\sin\gamma+\lambda^2)^{1/2}\right\}-2\sin\gamma\,\theta_2, \tag{14c}$$

where

$$\tan \theta_1 = \frac{\lambda \cos \gamma}{1 + \lambda \sin \gamma} ,$$

and

$$\tan \theta_2 = \frac{\frac{\lambda}{2} \cos \gamma + (1+2 \lambda \sin \gamma + \lambda^2)^{1/4} \sin (\theta_1/2)}{1 + \frac{\lambda}{2} \sin \gamma + (1+2 \lambda \sin \gamma + \lambda^2)^{1/4} \cos (\theta_1/2)} . \quad (14d)$$

It can be shown that the complete solution of the boundary value problem outlined in (5) is of the form

$$w = u - iv = A + B + i \frac{D}{\zeta - 1} + E w_2 \quad (15)$$

where A , B , D, E are real constants. On the unit circle the imaginary part of w is found to be

$$-v = B - \frac{D}{2} + Ex .$$

The normal velocity v is known from Eqs. (4) and (6) so that B , D , E can be found in terms of V_2 and Ω . Far downstream the velocity function approaches the known value

$$\lim_{x \to \infty} w = V_2 e^{-i\alpha_2} = A + iB + iEG ,$$

and A , B , E are now known in terms of α_2 , V_2 . The constants A, B, D, E, can now be eliminated and the velocity function becomes finally

$$w = V_2 \cos \alpha_2 - iV_2 (\sin \alpha_2 + \frac{\Omega G}{c}) - i \frac{2V_2 (\sin \alpha_2 + \frac{\Omega G}{c} - \frac{\Omega}{2})}{\zeta - 1} + V_2 \frac{\Omega}{c} w_2 . \quad (16)$$

As yet, the connection between α_1 , α_2 , V_1 and V_2 is not determined. The last relation is obtained from the remaining condition, namely, $w \to V_1 e^{-i\alpha_1}$, as $\zeta \to \zeta_1$. Equation (16) satisfies all boundary conditions,

is regular except for a leading edge singularity, and is therefore the sought-for solution. In the following paragraphs, explicit expressions for the leaving quantities, a_2 , V_2 will be found as a function of the entering quantities a_1 , V_1 and Ω. It is convenient to accomplish this result by forming the difference between the upstream and downstream conjugate velocities

$$V_1 e^{-i\alpha_1} - V_2 e^{-i\alpha_2} = -i\frac{2V_2\left\{\sin\alpha_2+\Omega\left(\frac{G}{c}-\frac{1}{2}\right)\right\}}{\zeta_1^{-1}} + 2iV_2\frac{\Omega}{c}\left\{e^{i\gamma}\,\delta n\,\frac{\zeta_1-\zeta_2}{\zeta_1}\right.$$

$$\left. + e^{-i\gamma}\,\delta n\,\frac{\zeta_1-\zeta_2}{\zeta_1}\right\} \qquad (17)$$

The relation

$$\frac{1}{\zeta_1}-1 = \frac{1}{2}\left[\sqrt{1+4\lambda}-1\right] = \frac{1}{2}\left[\left\{1+2\lambda\sin\gamma+\lambda^2\right\}^{1/4}\cos\frac{\theta_1}{2}-1 \;\; -i\left\{(1+2\lambda\sin\gamma+\lambda^2)^{\frac{1}{4}}\sin\frac{\theta_1}{2}\right.\right.$$

enables (17) to be separated (after considerable manipulation) into its real and imaginary parts:

$$V_1\cos\alpha_1 - V_2\cos\alpha_2 = -V_2\left[\sin\alpha_2+\Omega\left(\frac{G}{c}-\frac{1}{2}\right)\right](1+2\lambda\sin\gamma-\lambda^2)^{\frac{1}{4}}\sin\frac{\theta_1}{2} + a_1V_2 \qquad (17b)$$

$$V_1\sin\alpha_1 + V_2\sin\alpha_2 = -V_2\left[\sin\alpha_2+\Omega\left(\frac{G}{c}-\frac{1}{2}\right)\right]\left[(1+2\lambda\sin\gamma+\lambda^2)^{\frac{1}{4}}\cos\frac{\theta_1}{2}-1\right] + a_2V_2 \qquad (17c)$$

in which the substitutions

$$a_1 = -\frac{\Omega}{\pi G}\left\{\sin\gamma\left[\delta n(1-g)-\frac{1}{2}\delta n(1+2g\cos2(\gamma+\theta_2)+g^2)\right] + \cos\gamma\tan^{-1}\frac{g\sin2(\gamma-\theta_2)}{1+g\cos2(\gamma+\theta_2)}\right\}, \qquad (17d)$$

$$a_2 = \frac{\Omega}{\pi c}\left\{\cos\gamma\left[g\ln(1-g)+\frac{1}{2}\ln\left(1+2g\cos 2(\gamma+\theta_2)+g^2\right)\right] + \sin\gamma\tan^{-1}\frac{g\sin 2(\gamma+\theta_2)}{1+g\cos 2(\gamma+\theta_2)}\right\} \tag{17a}$$

and

$$g = \left(\frac{\lambda}{4}\right)^2\Big/\left\{1+\lambda\sin\gamma+\frac{\lambda^2}{4}+(1+2\lambda\sin\gamma+\lambda^2)^{\frac{1}{2}}\left(\lambda\sin\left(\gamma+\frac{\theta_1}{2}\right)+2\cos\frac{\theta_1}{2}\right)+\right.$$
$$\left.+(1+2\lambda\sin\gamma+\lambda^2)^{\frac{1}{2}}\right\} \tag{17b}$$

have been made.

In order to avoid endless repetition, the following auxiliary quantities are also introduced:

$$\left.\begin{aligned} b_1 &= (1+2\lambda\sin\gamma+\lambda^2)^{1/4}\sin\left(\frac{\theta_1}{2}\right)\\ e_1 &= b_1\,\Omega\left(\frac{\Omega}{2\pi c}-\frac{1}{2}\right)\\ b_2 &= (1+2\lambda\sin\gamma+\lambda^2)^{1/4}\cos\frac{\theta_1}{2}-1 = b_2'-1\\ e_2 &= b_2\,\Omega\left(\frac{\Omega}{2\pi c}-\frac{1}{2}\right)\\ d_2 &= a_2-e_2,\quad a_1-e_1 = c_1 \end{aligned}\right\} \tag{18}$$

After tedious reduction, the leaving angle α_2 is found to be

$$\sin\alpha_2 = +\frac{(b_1\tan\alpha_1+b_2')(d_2+d_1\tan\alpha_1)}{\tan^2\alpha_1+(b_1\tan\alpha_1+b_2')^2} +$$
$$+\sqrt{\frac{(b_1\tan\alpha_1+b_2')^2(d_2+d_1\tan\alpha_1)^2}{\left[\tan^2\alpha_1+(b_1\tan\alpha_1+b_2')^2\right]^2}-\frac{(d_2+d_1\tan\alpha_1)^2-\tan^2\alpha_1}{\tan^2\alpha_1+(b_1\tan\alpha_1+b_2')^2}} \tag{19}$$

The constants b_2, b_2', d_1, d_2, etc. are determined when γ, σ, and Ω are fixed. Thus (19) gives the leaving angle as a fairly complicated function of the inlet angle α. The ratio of inlet to outlet velocity is found from (17e), and is

$$\frac{V_1}{V_2} = \frac{\sin \alpha_2}{\sin \alpha_1} b_2' - \frac{d_2}{\sin \alpha_1} \quad . \tag{20}$$

These equations constitute the formal solution to the problem outlined in Section (II). Pressure distributions, cavity shapes, and other information can be computed, although only at the expense of considerable labor. It is, however, of particular importance to have expressions for the force coefficients, and this topic is treated next.

V. Normal Force and Drag Coefficients

The component of force normal to the chord line is

$$dF_N = (p-p_2)dx$$

from which the normal force coefficient C_N is obtained

$$C_N = \frac{F_N}{\rho V_1^2 c/2} = \frac{1}{c} \int_0^c c_p \, dx \tag{21}$$

Since $u' = u - V_2 \cos \alpha_2$ the force coefficient becomes

$$C_N = -\frac{2V_2 \cos \alpha_2}{c V_1^2} \int_0^c (u - V_2 \cos \alpha_2) \, dx \quad .$$

Furthermore, the fact that u = real w and $dz = dx$ on the slit, enables this coefficient to be written as

$$C_N = \frac{2V_2^2 \cos^2 \alpha_2}{V_1^2} - \frac{2V_2 \cos \alpha_2}{c V_1^2} \operatorname{Re} \int_0^c w dx \qquad (22)$$

where Re denotes that the real part of the integral is to be taken. To calculate C_N, the integral

$$J = \oint_\Gamma w dx$$

taken around the rhombic contour Γ enclosing one strip of the cascade (see Fig. 4) is first evaluated. From Section (IV) it can be determined that w is integrable on Γ and possesses no poles within it. Thus, $J = 0$. Furthermore, because of the periodicity of w the contributions to J from sections c-R, S-c' and O'-S', R'-O cancel. The remaining four terms of J are symbolically written as

$$J = 0 = \int_O^c + \int_R^S + \int_{c'}^{O'} + \int_{S'}^{R'} w dx .$$

Each of the terms other than the first is easily evaluated, since over their respective paths of integration w is constant (or at least the real part is). The real part of J is then used in conjunction with (22) to obtain the following simple formula for the normal force coefficient:

$$C_N = \frac{2}{\sigma} \frac{V_2 \cos \alpha_2}{V_1^2} \left\{ V_1 \sin(\gamma + \alpha_1) - V_2 \sin(\gamma + \alpha_2) \right\} \qquad (23)$$

The drag coefficient (defined as the force parallel to the chord line) can be found similarly:

$$C_D = \frac{1}{c} \int_0^c - c_p \, d\eta$$

or with (3) and (4)

$$C_D = \frac{2\cos\alpha_2}{c V_1^2} \int_0^c u' v dx = \frac{2\cos\alpha_2}{c V_1^2} \int_0^c u' (V_2 \sin\alpha_2 + v') dx \ .$$

This expression is easily converted into the form

$$C_D = - C_N \sin\alpha_2 - \frac{\cos\alpha_2}{c V_1^2} \mathrm{Im} \int_0^c w'^2 dz \qquad (24)$$

where

$$w' = w - V_2 e^{-i\alpha_2}$$

and Im indicates that the imaginary part of the integral is to be used. It can be shown that when the procedure followed above for the lift coefficient is used with Eq. (24), the drag coefficient becomes

$$C_D = - C_N \sin\alpha_2 + \frac{\cos\alpha_2}{\sigma} \left\{ \cos(\gamma+2\alpha_1) - 2\frac{V_2}{V_1} \cos(\gamma+\alpha_1+\alpha_2) + \left(\frac{V_2}{V_1}\right)^2 \cos(\gamma+2\alpha_2) \right\} \qquad (25)$$

This section completes the formal presentation of the theory, and in the next section several special cases are discussed.

VI. The Flat Plate Cascade

The exact solution of this problem by Betz has been previously mentioned, and it is taken up in the present section only to compare the results of the linearized theory with those of the exact theory for cascade flows. The pertinent formula for a flat plate cascade is obtained by setting $\Omega = 0$ in (16) and (17), and needless to say, considerable simplification ensues. For example, Eqs. (17b) and (17c) can be combined to give the two relations

$$2\cos\alpha_2 = \cos\alpha_1\left(\frac{V_2}{V_1}+\frac{V_1}{V_2}\right)+\sin\alpha_1\tan(\alpha_1+\gamma)\left(\frac{V_2}{V_1}-\frac{V_1}{V_2}\right) \tag{26}$$

and

$$\lambda = \frac{\sin\alpha_1\cos\alpha_1}{\sin^2\alpha_2\cos\gamma}\left(1-\frac{V_1^2}{V_2^2}\right)\left(1+\tan\alpha_1\tan(\gamma+\alpha_1)\right) . \tag{27}$$

The second of these gives the relation between the solidity (with the help of (9)) and the angles and velocity components. The first equation involves only a connection between the velocity ratio, stagger angle, inlet and discharge angle. Thus, given α_1 , γ , and V_1/V_2 , the leaving angle α_2 can be found from (26). The corresponding value of λ (and hence solidity) and normal force coefficient are then easily found.

Equation (26) is particularly interesting in that it can be obtained directly from the momentum principle by elementary computation. The flow is, of course, frictionless and there can be no drag force parallel to the plate. This fact, when used with the momentum law, results immediately in Eq. (26). The functional agreement of this result from a linearized theory with the exact momentum calculation is fortuitous in that, strictly speaking, all terms of order (α_2^2) or larger must be dropped to satisfy the constant pressure condition on the cavity. Nevertheless, the linearized theory should reflect accurately the condition of no drag on the flat plate even for rather large values of α_1 , since this is a physical requirement on the flow. The normal force coefficient may, however, depart appreciably from the exact result without violating this requirement. Values of V_1/V_2 were calculated and plotted vs. σ for $\alpha_1 = 3^\circ$ and 6° in Figs. 5 and 6. Normal force coefficients for these angles are presented in Figs. 7 and 8. It can be seen from these charts

that the velocity ratio V_1/V_2 is predicted quite well by the linearized theory. For example, at a given value of solidity the ratio of inlet to outlet velocity computed by this theory agrees to within 0.1 per cent of the exact theory. However, the situation is not nearly so favorable for the normal force coefficient. At small values of stagger angle, say, less than 45°, the agreement is about what one finds for isolated airfoil theory (given by $\sigma = 0$). But for values of $\gamma = 75^\circ$, the agreement is only fair -- even for solidities of one-half or less. In fact, for $\alpha_1 = 6^\circ$, $\sigma = 0.5$ and $\gamma = 75^\circ$, the linear theory overestimates the normal force coefficient by about forty per cent![*]

The present results for the flat plate are essentially the same as the choked flow calculations given by Cohen and Sutherland[4] except for minor differences in approximation of the cavitation number and definition of the stagger angle. In their work, the "stagger" angle used in the basic transformation is the geometric stagger angle previously defined plus the inlet angle α_1. The difference is small for small γ but for $\gamma = 70^\circ$, it becomes of first order in α_1 and can therefore be appreciable. From the foregoing study of the cavitating flat plate cascade, it can be seen that the linearized theory is a relatively good guide provided the inlet angle α_1 is not too large or the stagger angle is not too large.

VII. Smooth Entry for the Circular Arc

A feature of interest in the application of either fully wetted or

---

[*] If the alternative procedure of aligning the slit axis with the ultimate jet direction had been followed, the error would be smaller. The normal force coefficient for this case can be obtained from the charts of Figs. 7 and 8 by replacing γ by $\gamma + \alpha_2$.

cavitating hydrofoils is the angle of attack for the so-called "smooth entry" condition. In fully wetted flow this condition is said to occur when the leading edge singularity vanishes, for then the stagnation point lies at the leading edge. At any other angle of attack, infinite velocities occur at the nose if the nose is pointed. Of course, in no event do infinite velocities actually occur at the leading edge of a fully cavitated hydrofoil. However, in the linearized theory of flat plate hydrofoils a one-quarter order singularity is required there. Knowledge of the angle of attack for which this singularity vanishes is of interest to the designer since cavitation will commence on the lower or normally wetted side of the profile for smaller incidence angles. For this reason, the value of α_1 for which smooth entry occurs is said to be the "design" angle of attack herein.

Smooth entry takes place when the coefficient of $1/(\zeta-1)$ in Eq. (16) vanishes, and evidently this occurs when

$$\sin \alpha_2 = \left(\frac{1}{2} - \frac{G}{2\pi} \right). \tag{28}$$

The inlet angle for smooth entry is found to be

$$\tan \alpha_1 = \frac{\sin \alpha_2 - a_2}{a_1 + \cos \alpha_2} \tag{29}$$

and the ratio of inlet to leaving velocity is

$$\frac{V_1}{V_2} = \left\{ (\sin \alpha_2 - a_2)^2 + (a_1 + \cos \alpha_2)^2 \right\}^{1/2} \tag{30}$$

It is of interest to compare the values of Eqs. (28) and (29) with known limiting conditions. The case of infinite solidity is particularly simple for then $\sigma \longrightarrow \infty$ and Eq. (29) gives the known limit $\alpha_1 = \Omega/2$. For the same condition, α_2 is found to be $-\Omega/2$, so that the flow is

"perfectly" guided. The results for zero solidity (or isolated foils) are obtained by putting $\sigma = 0$ into the above formulae. It is quickly found that this results in $\alpha_1 = \alpha_2$ (i.e., no turning of the flow) and $\alpha_1 = \Omega/8$ in agreement with the results of flow past isolated cavitating circular arc profiles at zero cavitation number. The angle of attack for smooth entry of the isolated cavitating circular arc may be contrasted to that of the fully wetted circular arc for which $\alpha_1 = 0$. In Fig. 9 the ratio of $\tan \alpha_1/\Omega$ is plotted vs σ for various values of γ and Ω. The effect of Ω is slight, as would be anticipated. The leaving angle α_2/Ω is plotted in Fig. 10 for the smooth entry condition, and is seen to be strongly dependent upon stagger angle and solidity. The trend with solidity, however, is similar to that of fully wetted flow in a cascade, and in fact, the deviation angle ($\delta = \frac{\Omega}{2} + \alpha_2$) for values of γ between 45 and 60 degrees can be estimated with an error of less than one in fifteen by a modified value of Constant's rule, i.e., $\delta = 0.24/\sqrt{\sigma}$ if σ lies between 0.5 and 1.5.

VIII. Discussion of Results

Of principal interest in this investigation is the behavior of the normal force coefficient with solidity and stagger angle. The calculation procedure, though straightforward, is quite tedious. The present computations obtained with the use of a desk calculator, are limited in scope and are intended to show only the general features of the problem. Figures 11 through 13 present normal force coefficients for stagger angles of 0, 45, and 60° respectively, and for values of σ nominally equal to 0.5, 1.0, and 1.5. It is immediately apparent that the influence of stagger angle and solidity are profound. Reference curves of C_N vs α_1 for an isolated circular arc hydrofoil are taken from Ref. (4), and are

also plotted on Figs. 11 through 13. It is seen that even for $\sigma = 0.5$ the value of the normal force coefficient is significantly different from its isolated value and that the amount of discrepancy increases as the stagger angle increases. Of course, these curves are not exactly comparable, since the cavitation number in cascade is not zero. This point is investigated for the case of $\gamma = 0$ (Fig. 11) by plotting the normal force coefficient for the isolated hydrofoil at the same cavitation number as that for $\sigma = 0.5$. It is seen that on this basis the discrepancy is even larger. A similar result is also found for $\gamma = 45$ and 60°, but is not shown.

The cavitation number of the flow described above is not arbitrary but is a function of the angle of attack and solidity as shown for the configurations studied in Figs. 14 a, b, c. Also shown on these graphs, as well as those of Figs. 11-13, is the locus of points for which smooth entry occurs. It is particularly interesting to note that extremely low cavitation numbers result for the large stagger angles. This finding is in keeping with the results of the flat plate calculations shown in Figs. 5, 6. A further interesting comparison between the flat plate and circular arc cavitating cascades is made in Table I below, with information taken from Figs. 5-15. It is quite clear from this tabulation that the use of camber results in lower cavitation numbers and greater normal force coefficients at the same inlet angle than experienced by the flat plate lattice. If this numerical comparison had been made at the same normal force coefficient, the superiority of the circular arc profile would have been even more apparent.

It can be seen from the graphs of Figs. 11-13 inclusive that even for the modest solidity of 0.5 the interference of adjacent blades in the castade would prevent reliable estimates to be made of the normal force

Table I.

Comparison of Circular Arc and Flat Plate Cascades at an Inlet Angle $\alpha_1 = 6^\circ$

Stagger Angle γ	Solidity σ	Circular Arc		Flat Plate	
		K	C_N	K	C_N
0	1.03	0.145	0.30	0.20	0.16
45	1.03	0.037	0.21	0.08	0.078
60	1.07	0.011	0.165	0.045	0.051

coefficient on the basis of isolated hydrofoil theories. This conclusion, however, takes no account of the turning of the flow as it passes through the cascade. As in the case of fully wetted cascade flow, it is likely that the significant velocity vector in determining the force on an individual blade is the vector mean of the inlet and outlet velocities. In fact, in fully wetted flow, when the normal force coefficient is based on the vector mean velocity and the angle of attack is taken as the angle between the chord and the vector mean velocity, little discrepancy from the isolated force coefficient is found until the solidity becomes about 0.5. It is reasonable to suppose, therefore, that a similar effect takes place in the cavitating cascade flow of the present work. With this view in mind, the normal force coefficients for the cases studied are given in Figs. 15, 16, 17, as a function of the algebraic average of the inlet and leaving angles, i.e., $(\alpha_1 + \alpha_2)/2$ -- a close approximation to the vector mean angle when α_1, α_2 and K are small. It is clear from these diagrams that the normal force coefficient so presented for $\gamma = 0$ agrees closely with the values for an isolated hydrofoil at the same cavitation number. Although some departure from the isolated result is observed for higher stagger angles, the agreement is still uniformly better on this

basis than with the inlet angle α_1. This observation is found to be particularly true for $\sigma = 0.5$ for all stagger angles when the comparison is made at the same cavitation number.*

Accurate calculations of the drag coefficient have not yet been made. Preliminary results of a rough nature for a stagger angle of zero indicate that the drag coefficient is always less than about two per cent of the normal force coefficient. The sign of this force is not constant, but is negative for the larger angles of attack and positive for small angles. It will be recalled that the "drag" force is defined herein to be parallel to the chord. Thus, the drag coefficient of a flat plate will be zero by the present convention. The drag coefficient of an isolated circular arc hydrofoil at zero cavitation number, when computed on the present basis, shows a behavior similar to that observed for the cascade, but is of somewhat greater magnitude. Further discussion of this interesting point must await numerical computations now in progress.

Extensions: An important feature yet to be determined is the effect of cavities of finite length, and for this purpose several models of the cavity closure may be used as discussed at length by Parkin[4]. Probably the most straightforward procedure would be to use the fully closed cavity first used by Tulin[3] and also by Cohen and Sutherland in their work on the flat plate cascade. However, it is not completely clear which of the many models conceivable give rise to the simplest results for computation.

The case of the partially cavitating cascade is also of considerable

---

* This result suggests that the neglect of the interference effect and wake blockage in supercavitating propeller design is justified only for $\sigma \leq 0.5$

interest. Partial cavitation in a cascade of flat plates has been treated in Ref. (8), only for the case of semi-infinite plate length. The interest in this work was to obtain simple relations between the cavity proportions and the flow geometry for application to inducer pumps. Partial cavitation occurs frequently in the blades of conventional water pumps and propellers of more complex shape than treated in (8). It would be of great value to have such a case worked out in detail, and for a circular arc profile the present method could be used to advantage.

IX. Conclusion

A linearized theory has been presented of the cavitating flow through a cascade of circular arc hydrofoils. However, only the case of cavities of infinite length was treated. Normal force coefficients are given for a range of stagger angles and angles of attack for a camber of 16 degrees. Comparison of the results of the linear theory with an exact theory for flat plate cascades indicates that the theory is limited to values of the stagger angle of about 60 degrees -- at least for an angle of attack of 6 degrees. Solidity is observed to have a dominant effect on the normal force coefficient -- although, when the angle of attack is measured from the mean of the entering and leaving angles, the discrepancy from the results of isolated theories is sharply reduced. It is concluded that as a rule of thumb, no appreciable cascade effect occurs up to about a solidity of one half if the angle of attack is so determined.

REFERENCES

1. Betz, A. and Petersohn, E., "Application of the Theory of Free Jets," NACA TN 667, (April 1932).

2. Cornell, W. G., "The Stall Performance of Cascades," Proc. 2nd U. S. National Congress of Appl. Math., (June 1954), pp. 705-713.

3. Tulin, M. P., "Supercavitating Flow Past Foils and Struts," Paper No. 16, Symposium on Cavitation in Hydrodynamics (Sept. 1955), National Physical Laboratory, Teddington, England.

4. Parkin, B. R., "Linearized Theory of Cavity Flow in Two Dimensions," Report P-1745, the Rand Corporation, Santa Monica, California.

5. Cohen, H. and Gilbert, R., "Two Dimensional Steady Cavity Flow About Slender Bodies in Channels of Finite Breadth," Journal of App. Mech., Trans. ASME (Nov. 1956).

6. Cohen, H. and Sutherland, C. D., "Finite Cavity Cascade Flow," Math. Report No. 14, Rensselaer Polytechnic Institute, (April, 1958), Troy, New York.

7. König, E., "Potentialstromung durch Gitter," Ztsch. f. Angew. Math. u. Mech., Bd. 2, (1922).

8. Acosta, A. J. and Hollander, A., "Remarks on Cavitation in Turbomachines," Report No. 79-3, Eng. Div., California Institute of Technology, Pasadena, Calif. (Oct. 1959).

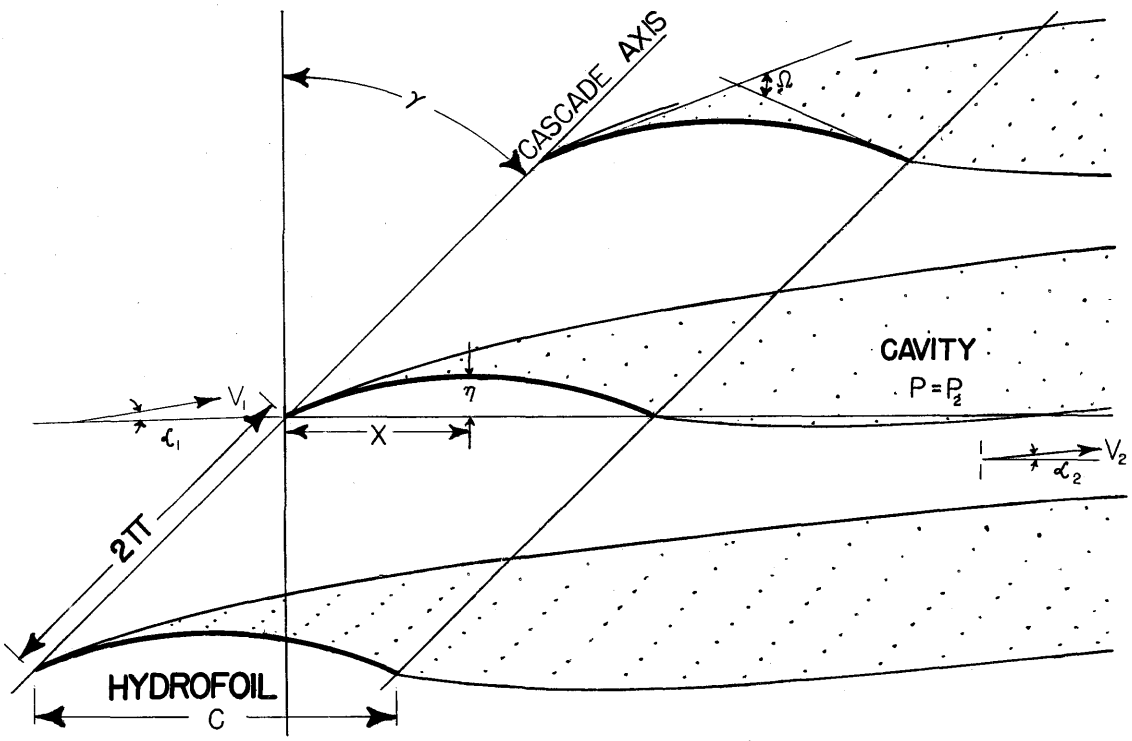

Fig. 1. Cascade of cavitating circular arc hydrofoils.

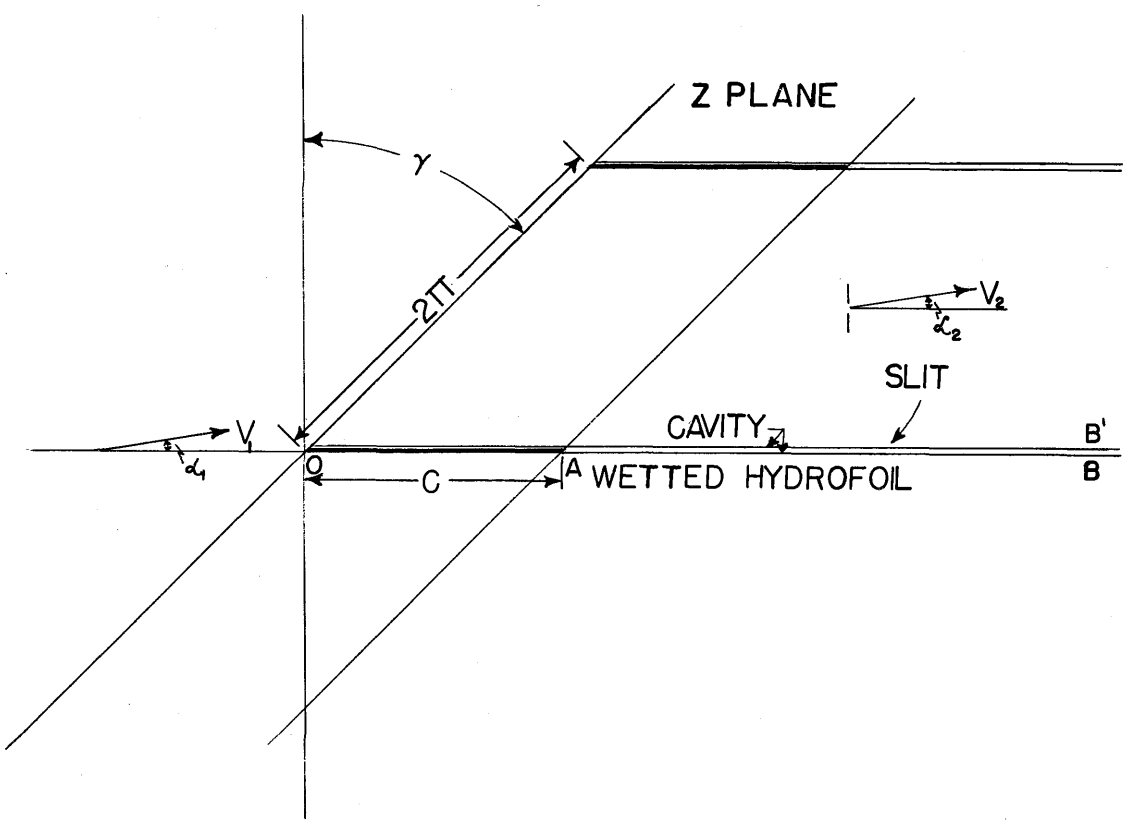

Fig. 2. Definition sketch of the physical (z) plane.

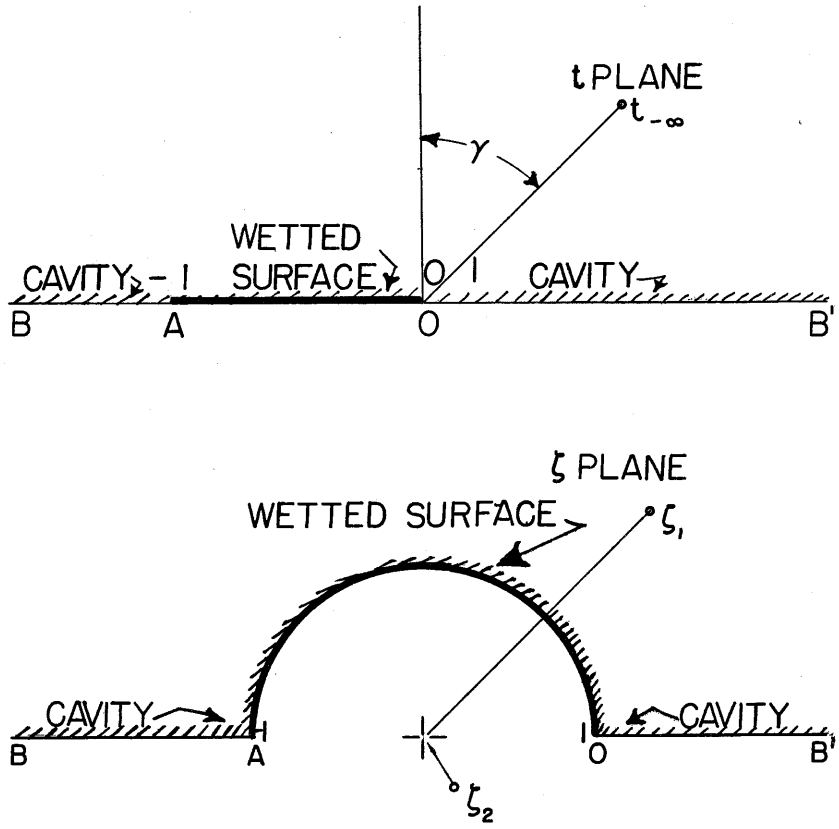

Fig. 3. Auxillary planes.

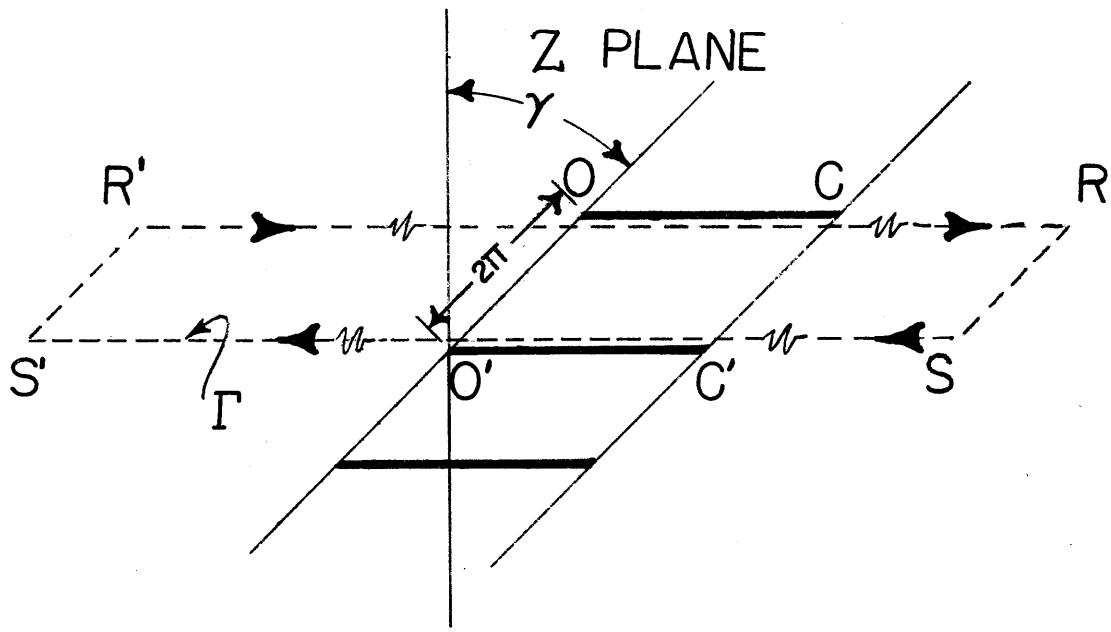

Fig. 4. Integration contour in the cascade plane.

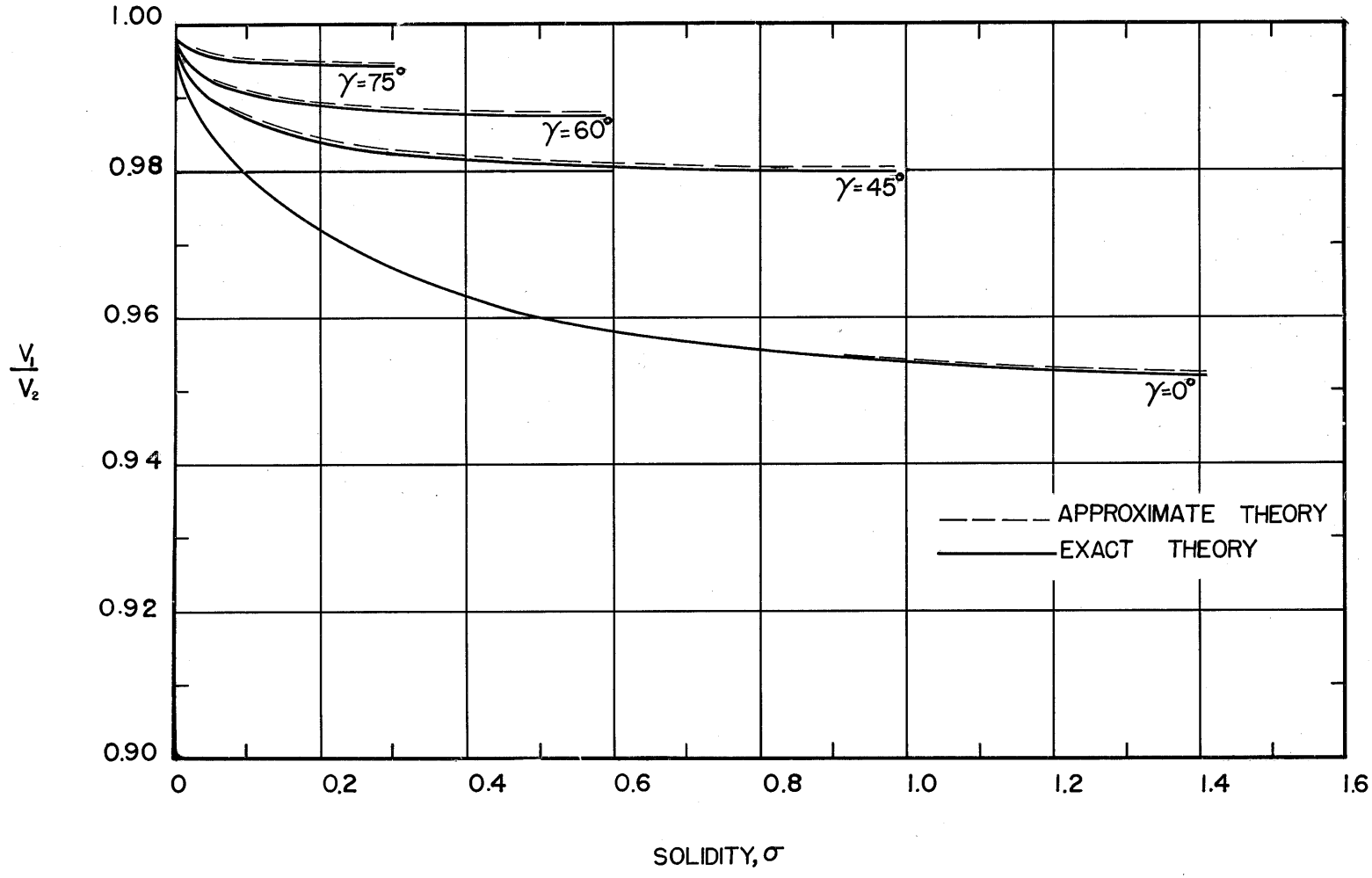

Fig. 5. Ratio of upstream to downstream velocity vs solidity for a fully cavitating cascade of flat plates with an inlet flow angle of 3°. The exact theory is computed from the results of Ref. 1.

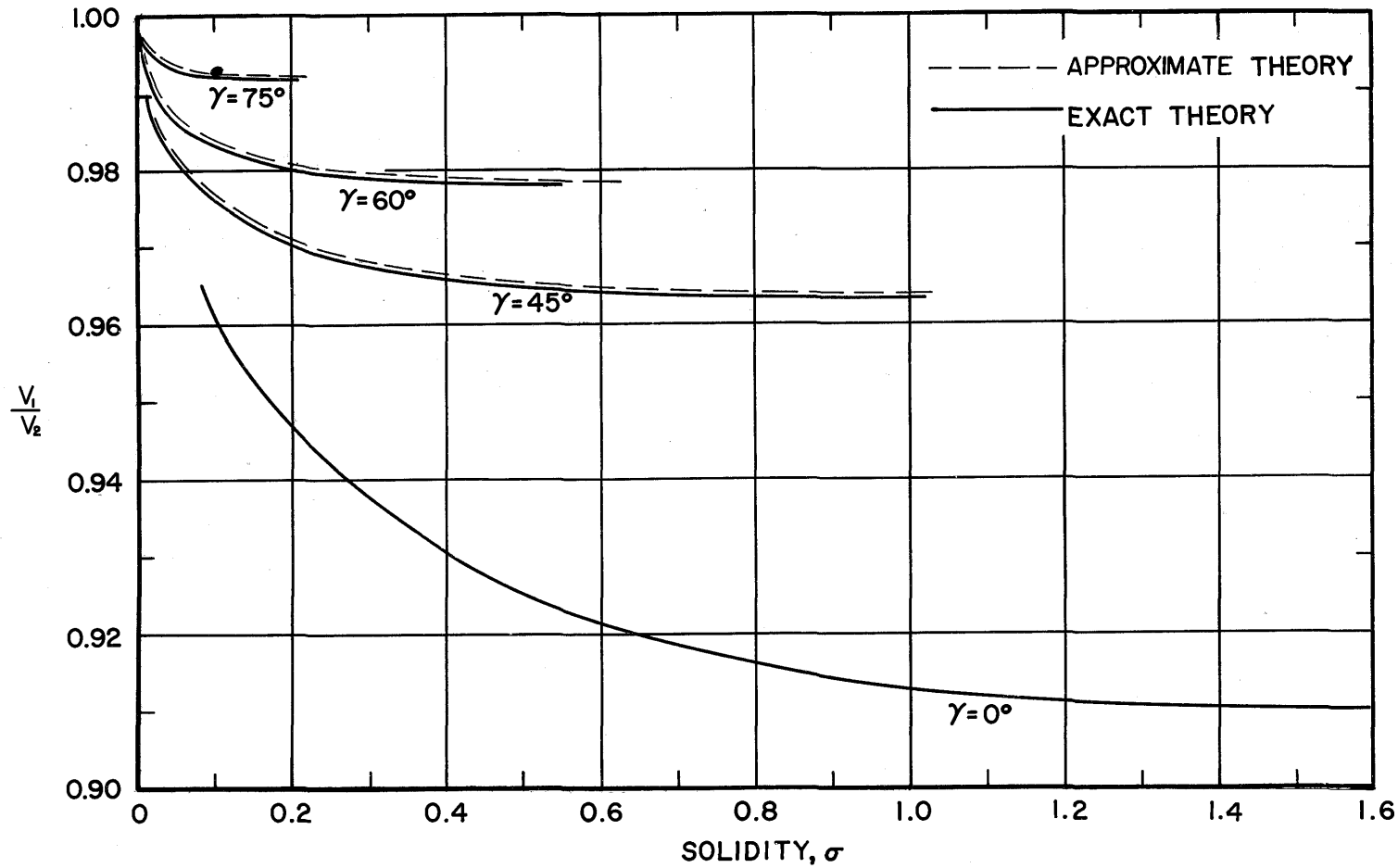

Fig. 6. Ratio of upstream to downstream velocity vs solidity for a fully cavitating cascade of flat plates with an inlet flow angle of 6°.

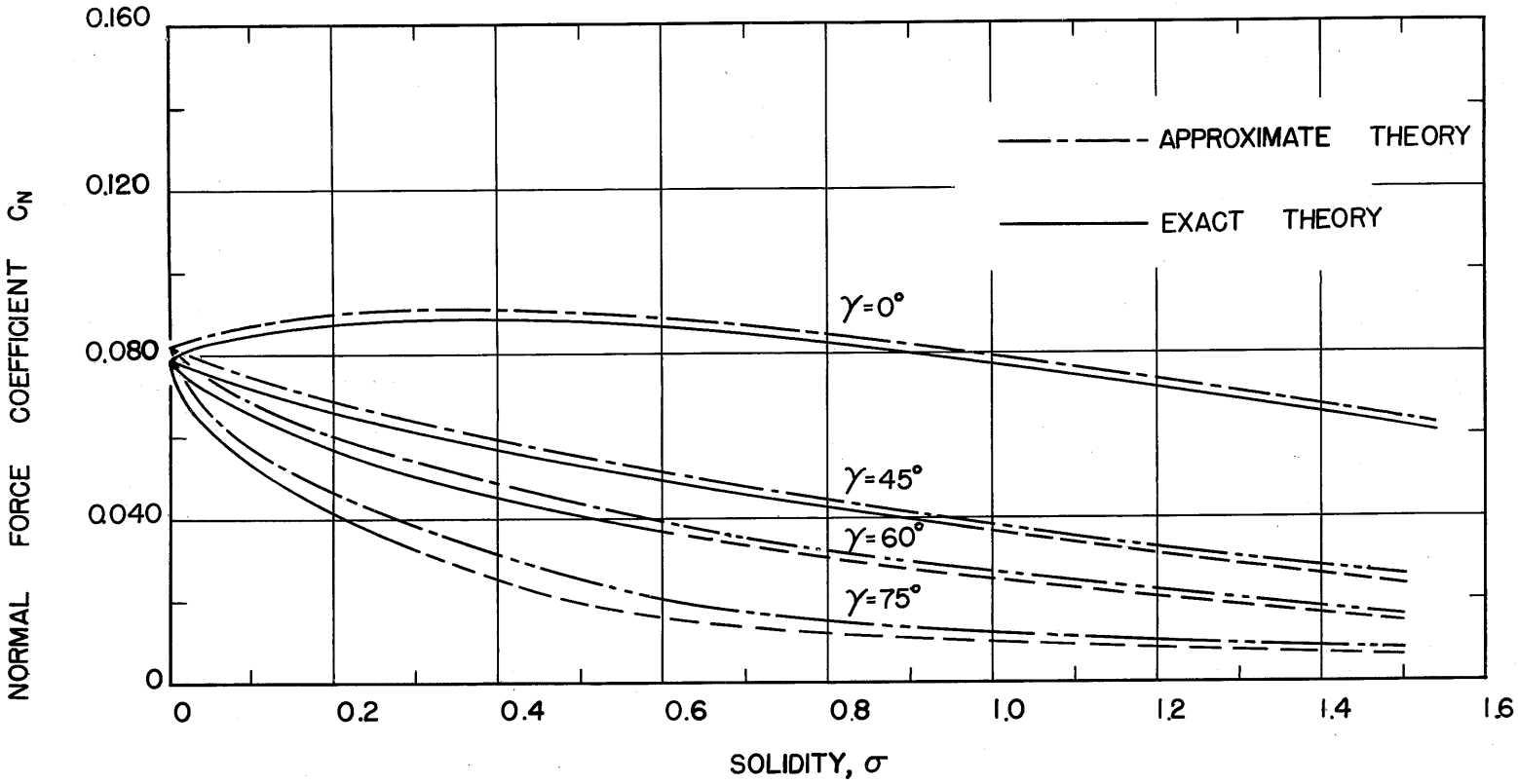

Fig. 7. Normal force coefficient vs solidity for a fully cavitating flat plate cascade with an inlet flow angle of 3°.

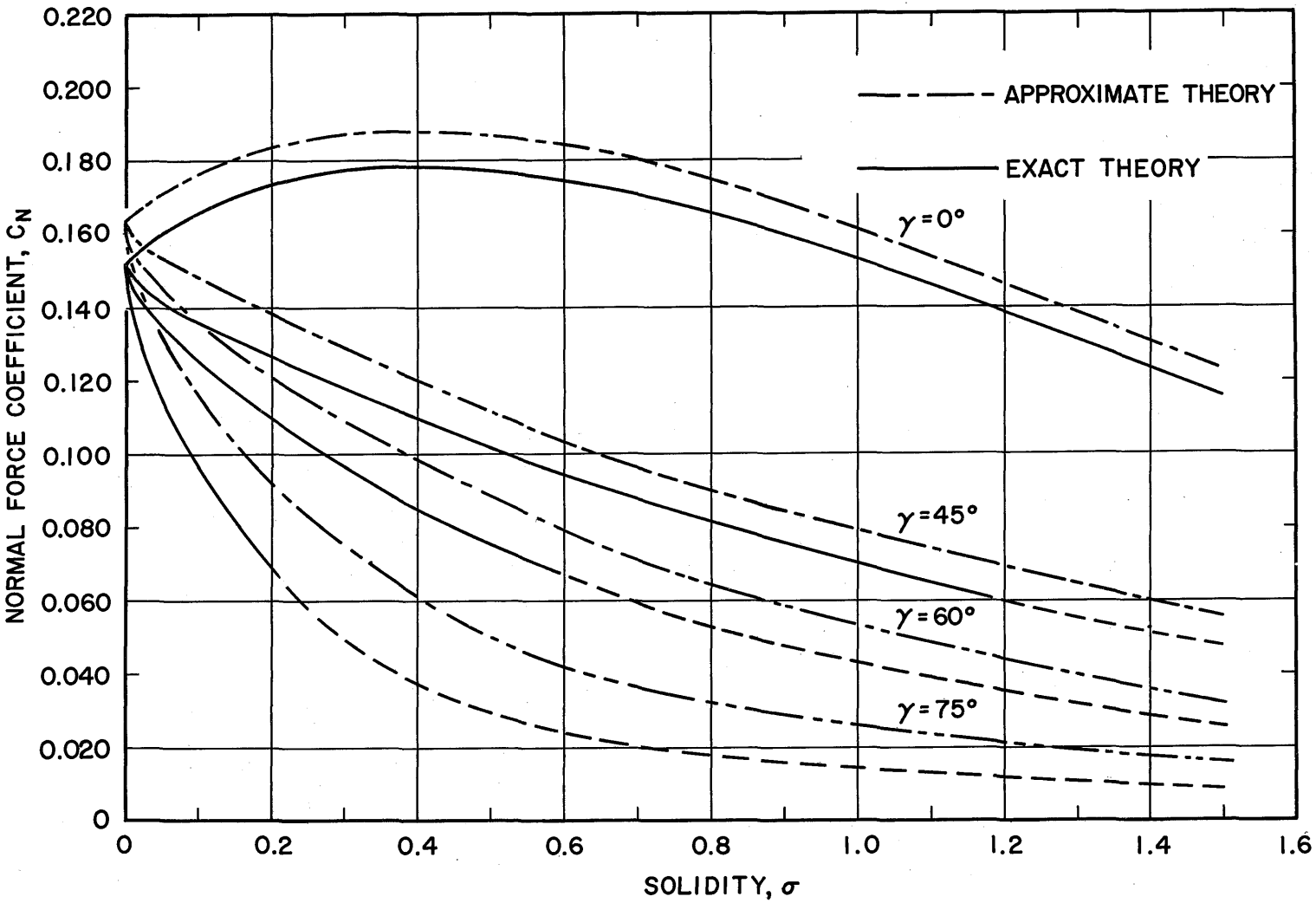

Fig. 8. Normal force coefficient vs solidity for a fully cavitating flat plate cascade with an inlet flow angle of 6°.

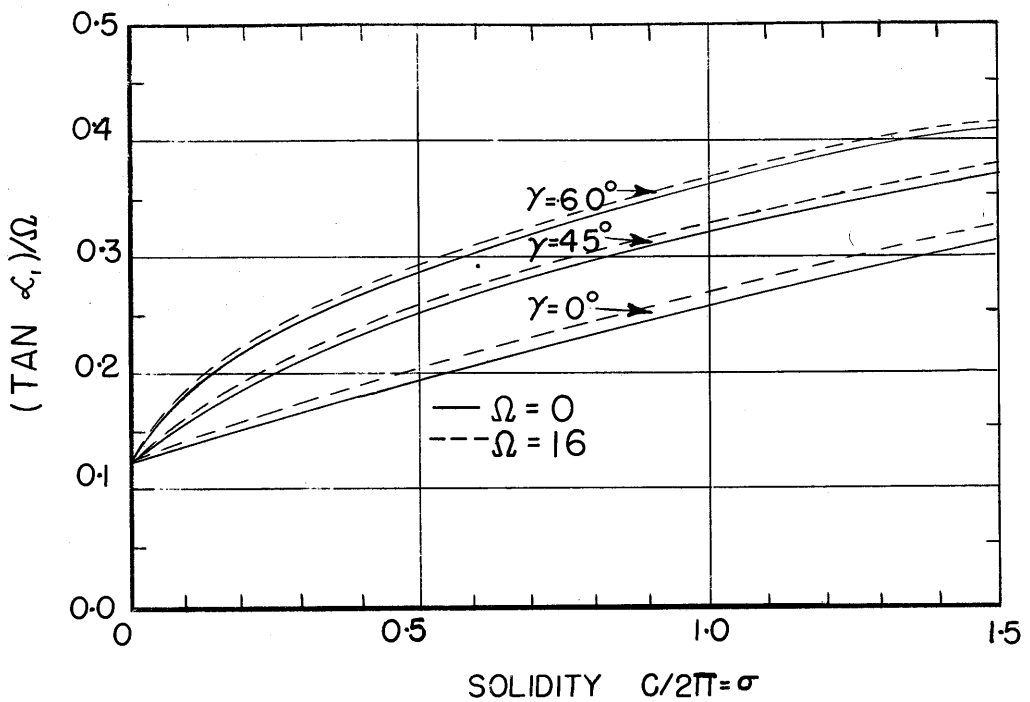

Fig. 9. Smooth entry or design condition for a cascade of fully cavitating circular arc hydrofoils.

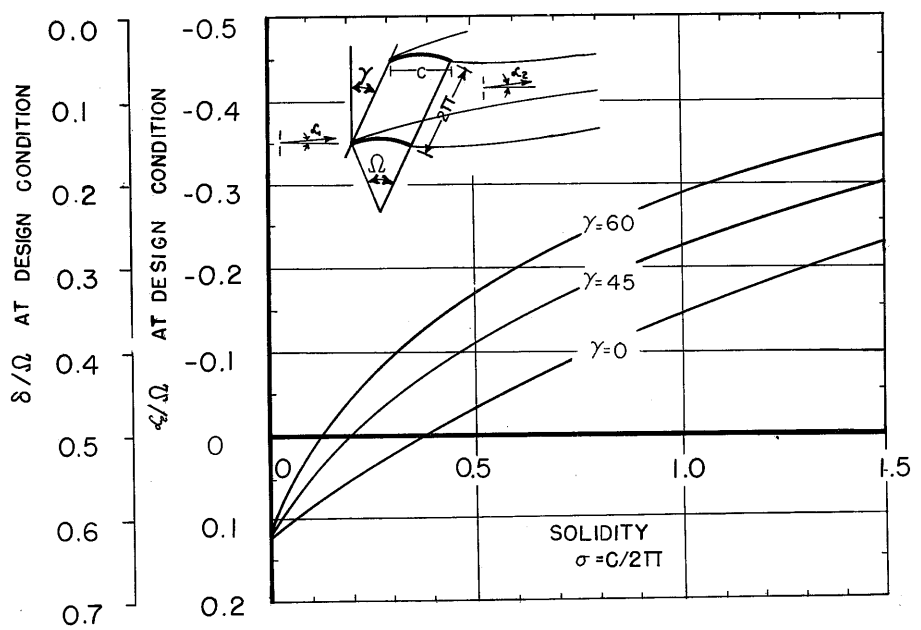

Fig. 10. Leaving angle and deviation angle vs solidity for a fully cavitating cascade of circular arc hydrofoils at the design condition ($\Omega = 16^{\circ}$).

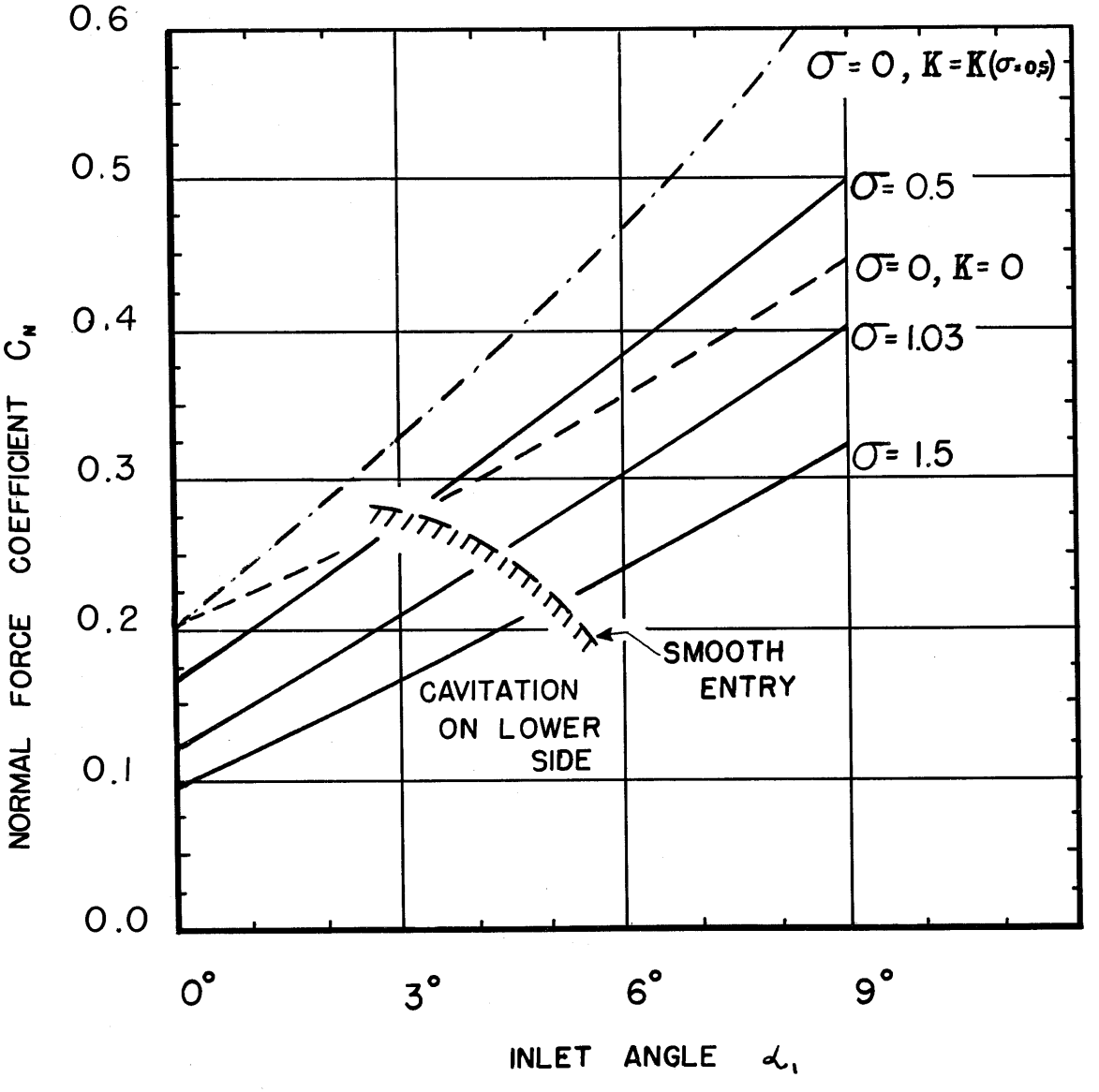

Fig. 11. Normal force coefficient vs inlet flow angle for a cascade of fully cavitating circular arc hydrofoils with a camber of 16° and for zero stagger angle.

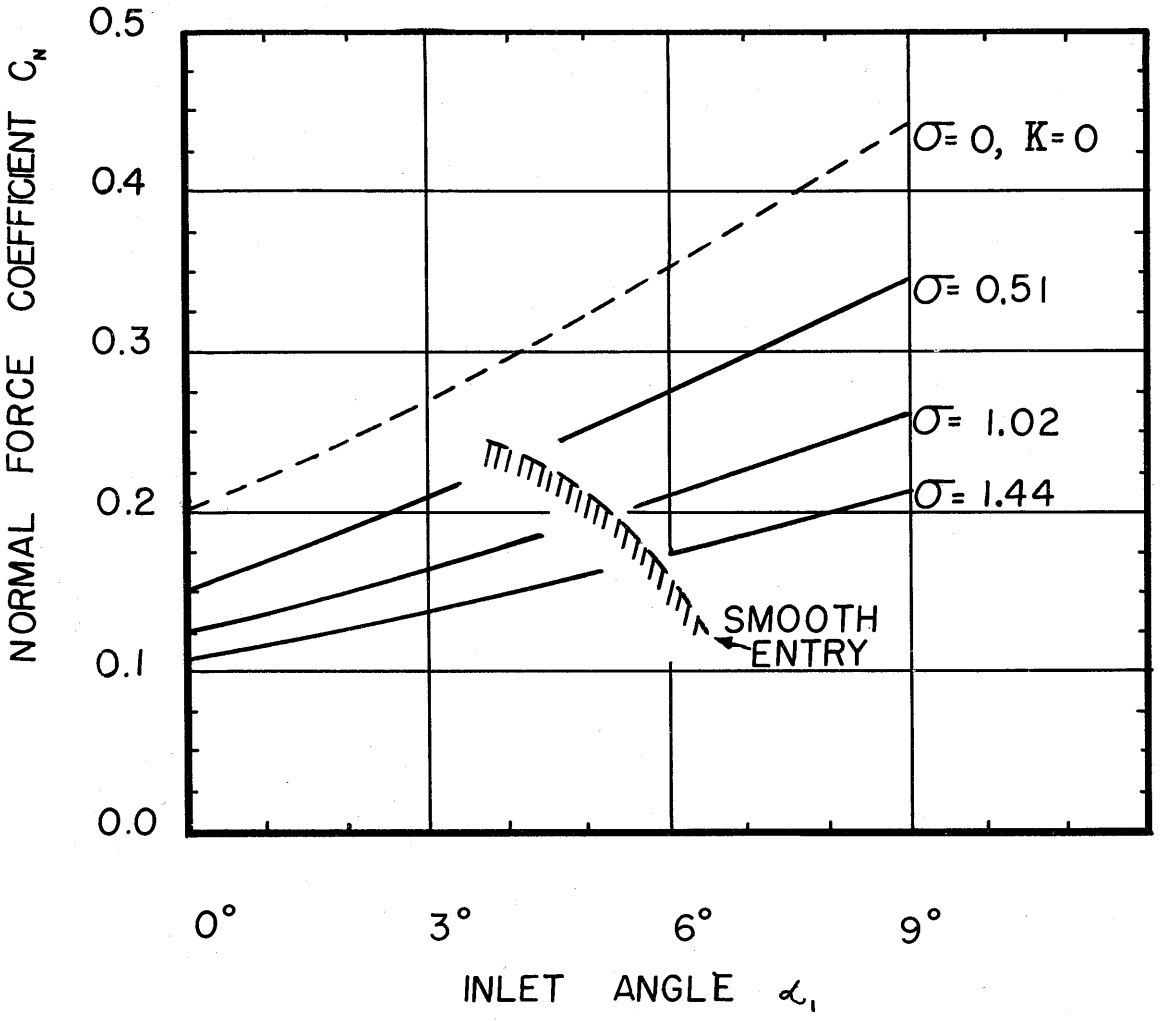

Fig. 12. Normal force coefficient vs inlet flow angle for a cascade of fully cavitating circular arc hydrofoils with a camber of 16° and 45° stagger angle.

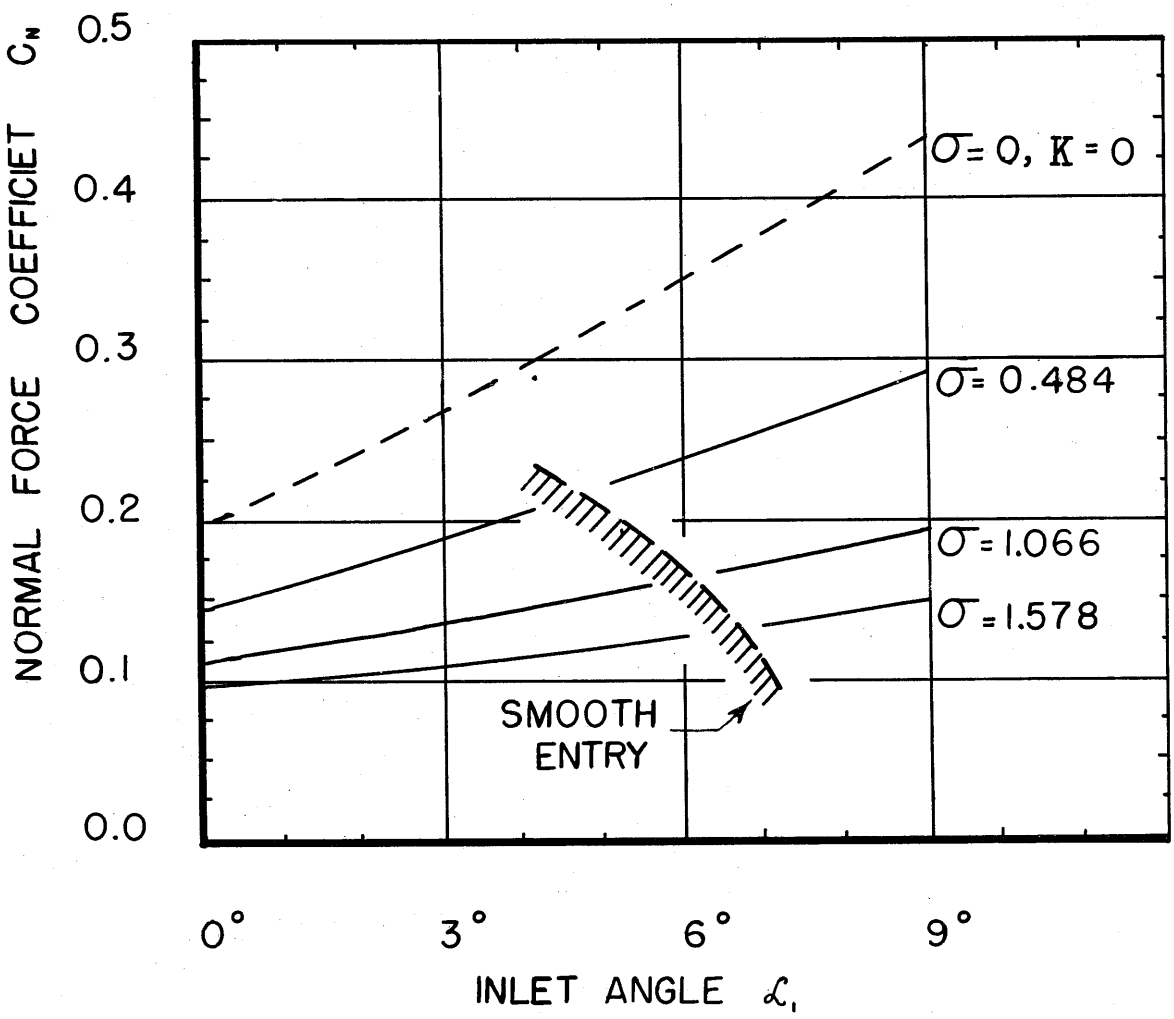

Fig. 13. Normal force coefficient vs. inlet flow angle for a cascade of fully cavitating circular arc hydrofoils with a camber of 16° and 60° stagger angle.

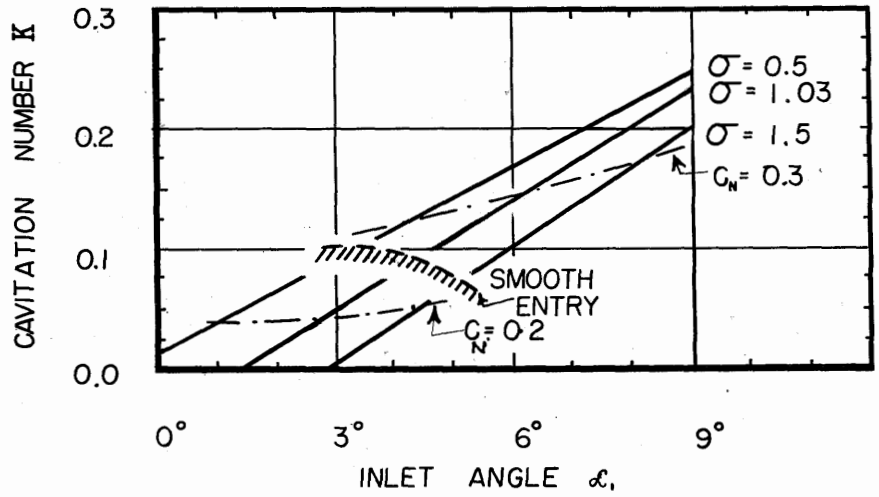

Fig. 14-a. $\gamma = 0^{\circ}$

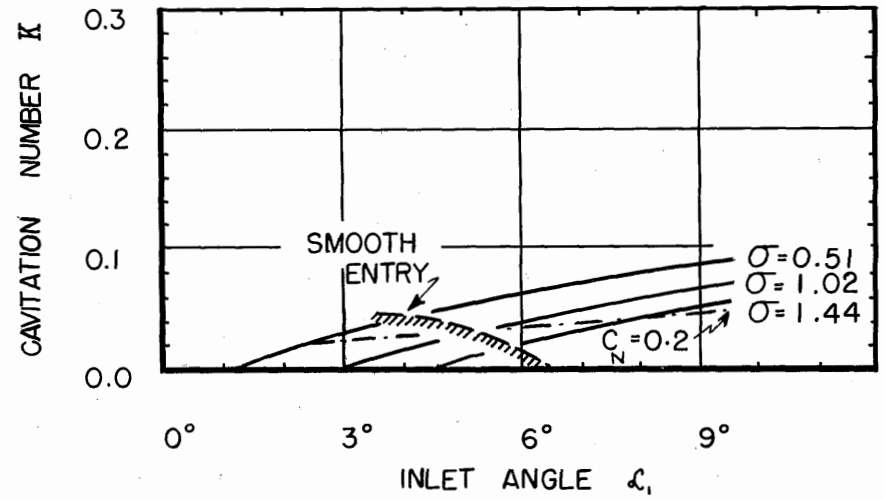

Fig. 14-b. $\gamma = 45^{\circ}$

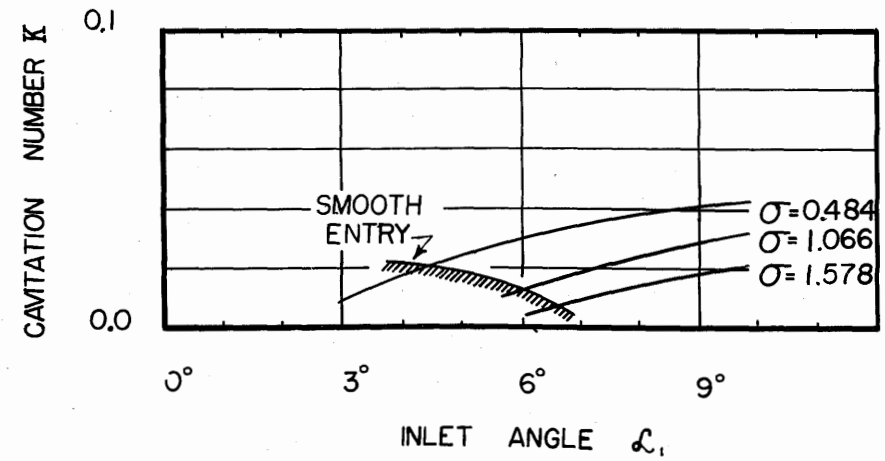

Fig. 14-c. $\gamma = 60^{\circ}$

Fig. 14. Choking or limiting cavitation number for a cavitating cascade of circular arc hydrofoils with a camber of 16°.

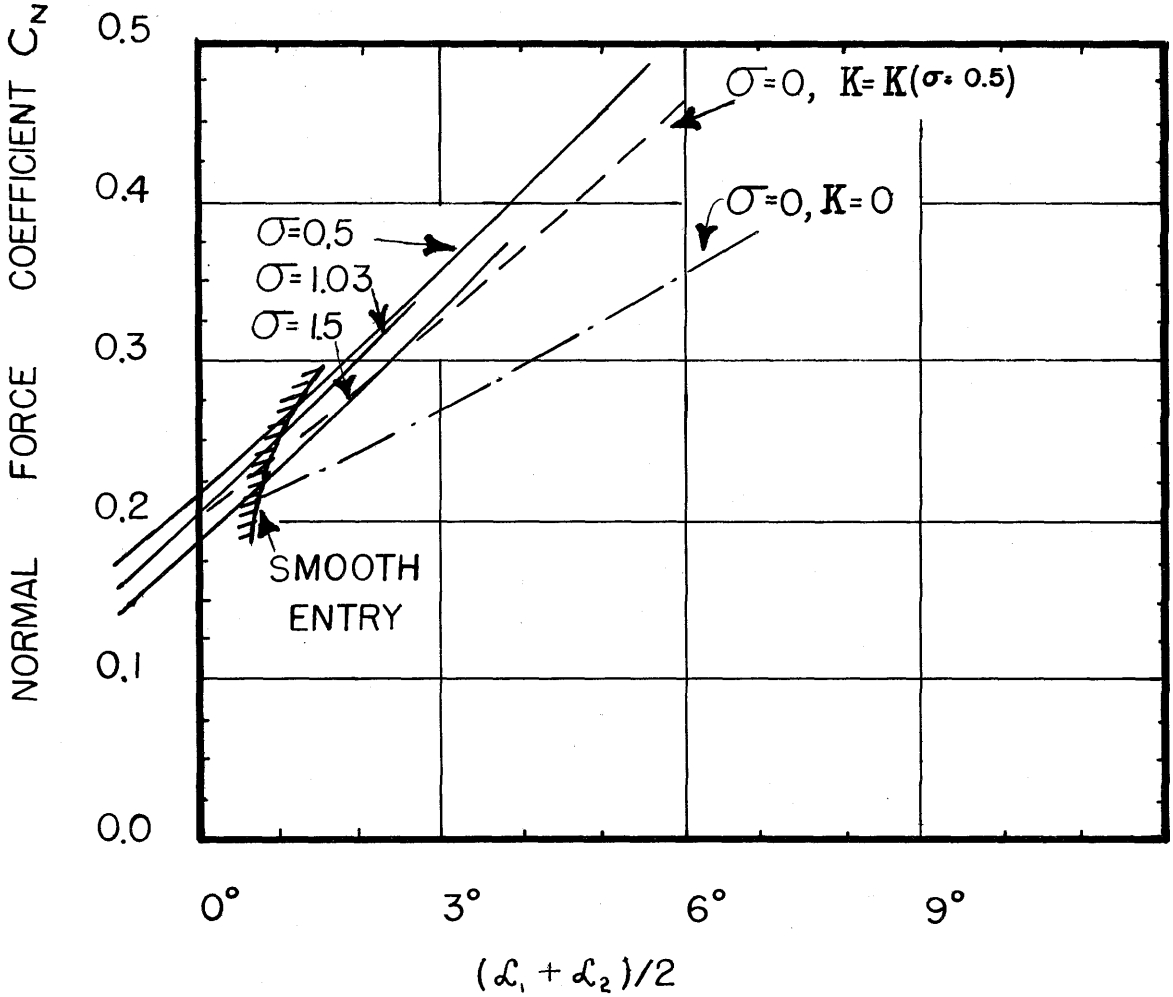

Fig. 15. Normal force coefficient vs mean of inlet and leaving flow angles for a cascade of cavitating circular arc hydrofoils with a camber of 16° and zero stagger angle.

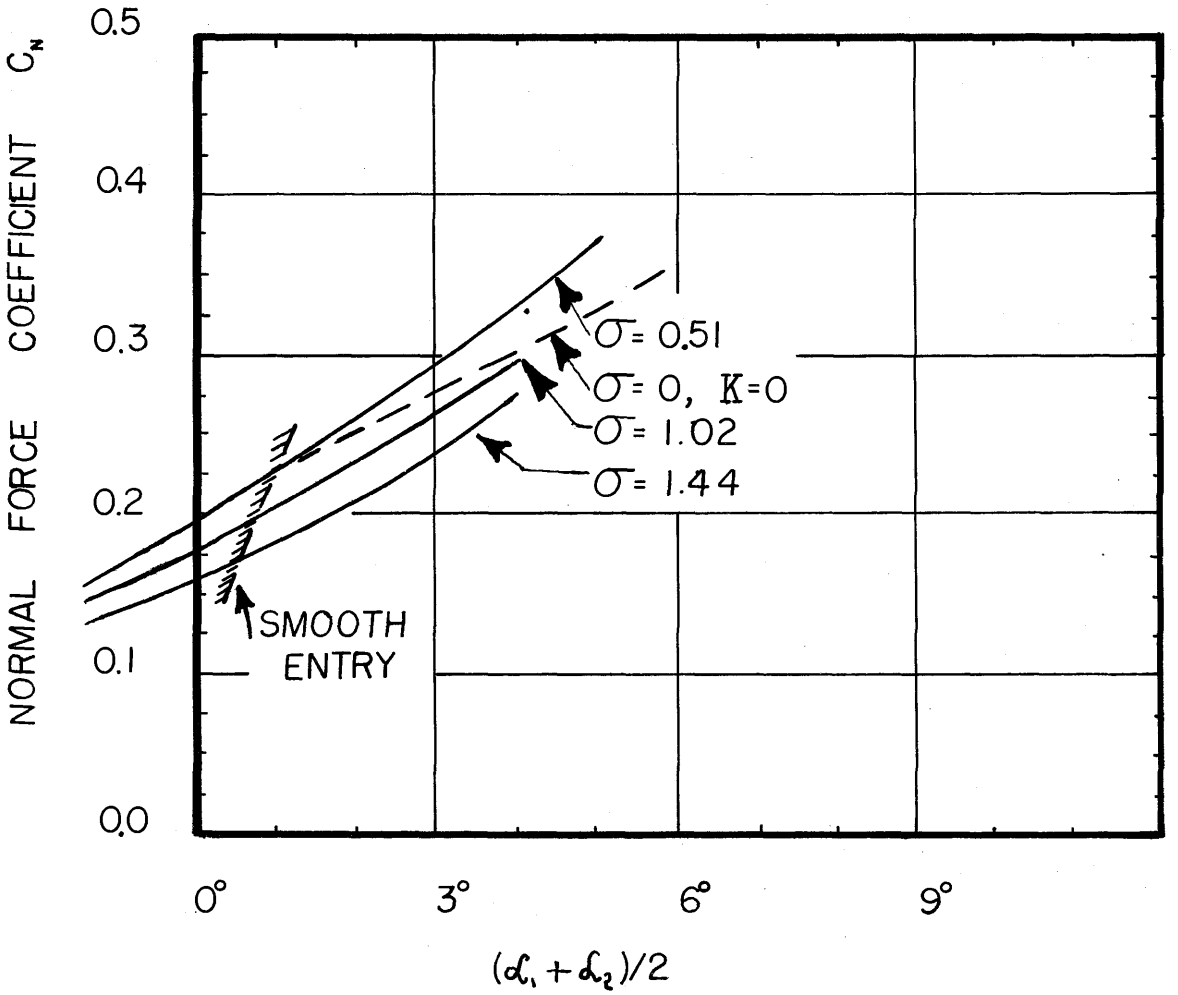

Fig. 16. Normal force coefficient vs mean of inlet and leaving flow angles for a cascade of cavitating circular arc hydrofoils with a camber of 16° and 45° stagger angle.

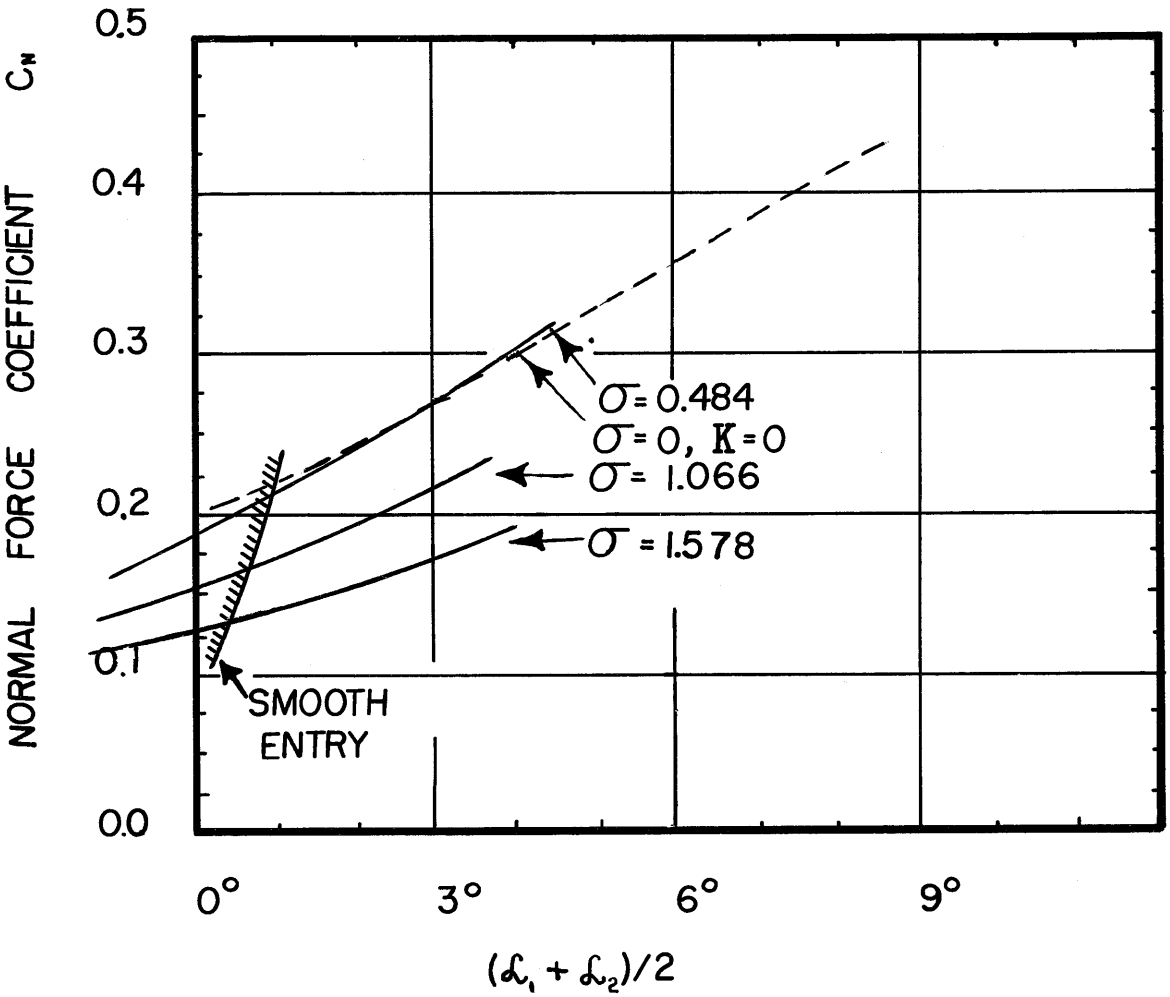

Fig. 17. Normal force coefficient vs mean of inlet and leaving flow angles for a cascade of cavitating circular arc hydrofoils with a camber of 16° and 60° stagger angle.